

# Efficient multi-qubit subspace rotations via topological quantum walks

Xiu Gu,<sup>1,\*</sup> Jonathan Allcock,<sup>1</sup> Shuoming An,<sup>1</sup> and Yu-xi Liu<sup>2,3</sup>

<sup>1</sup>*Tencent Quantum Laboratory, Tencent, Shenzhen, Guangdong 518057, China*

<sup>2</sup>*School of integrated circuits, Tsinghua University, Beijing 100084, China*

<sup>3</sup>*Frontier Science Center for Quantum Information, Beijing, China*

(Dated: November 15, 2021)

The quantum singular value transformation (QSVT) is a powerful framework encompassing a number of well-known quantum algorithms. A key requirement of QSVT is the ability to rotate a subspace by a chosen angle. This is usually implemented via multiple-controlled-phase gates, which leads to large circuit depth when decomposed into one- and two-qubit gates. Here, we propose a fast, high-fidelity way to implement such operations via topological quantum walks, where a sequence of single-qubit  $z$  rotations of an ancilla qubit are interleaved with the evolution of a system Hamiltonian in which a matrix  $A$  is embedded. The subspace spanned by the left (right) singular vectors of  $A$  is rotated depending on the state of the ancilla. This procedure can be implemented in a superconducting processor with star-type connectivity, significantly reducing the total gate time required compared to previous proposals.

*Introduction.*—The design and implementation of quantum algorithms are at the heart of attaining practical applications for quantum computing. The recently proposed quantum singular value transformation (QSVT) algorithm [1] is particularly powerful and general, and provides a unifying framework tying together other well-known algorithms such as quantum search, phase estimation, matrix inversion and Hamiltonian simulation [2]. Building on the frameworks of quantum signal processing and qubitization [3–5], in QSVT one interleaves projector-controlled phase shifts with a unitary operator which block encodes a matrix  $A$  to implement polynomial transformations of the singular values of  $A$ . Efficient implementation of such projector-controlled phase shifts, i.e. subspace rotations, is thus of central importance for carrying out QSVT.

The conventional way to implement subspace rotations is via the multiple-controlled-phase gate  $C_nZ$ , i.e. the gate on  $n+1$  qubits which effects the reflection  $\mathbb{I}-2|\psi\rangle\langle\psi|$ , with  $|\psi\rangle$  the state where all  $n+1$  qubits are  $|1\rangle$ . When sandwiched between unitary transformations, reflection about arbitrary states can be constructed [6, 7]. Rotation of a subspace by a chosen angle can then be implemented from two rounds of controlled-reflections surrounding a single-qubit rotation [2]. However,  $C_nZ$  gates require large circuit depth when decomposed into single- and two-qubit gates [8].

Quantum walks, in addition to forming powerful algorithms in their own rights [9, 10], are also useful tools for the digital simulation of single-particle topological band structure [11–13]. In this framework, the band-structure topology determines the Berry phase imprinted on the walker when it refocuses to its initial position after adiabatically traversing the Brillouin zone [12, 13].

In this Letter, we show how to implement reflections and rotations of a subspace based on topological quantum walks. This is achieved by embedding a matrix  $A$  in a block Hamiltonian  $H$ . The sequence of interleaving  $e^{-iHt}$

and single-qubit  $z$  rotations of an auxiliary qubit mimics discrete-time quantum walks with topological winding number one [11]. With the auxiliary qubit initialized in  $|0\rangle$  ( $|1\rangle$ ), the right (left) singular vectors acquire a phase of  $\pi$  due to the non-zero topological winding number. States which are not coupled to the qubit correspond to the topologically trivial phase, and acquire a phase determined by the sequence of single-qubit  $z$  rotations. Superconducting circuits [14–19] are among the leading platforms for quantum computers, and well suited to implementing our proposal. We show how this can be done in a superconducting system where a central ancilla qubit is coupled to four neighbors. Reflection and rotation operations are implemented by a topological quantum walk sequence, which alternates simultaneous CZ gates [20] between the ancilla and neighbor qubits and single-qubit  $z$  rotations of the ancilla.

*Topology of quantum walks.*—In a discrete-time quantum walk, the position of a particle is controlled by repeated application of the unitary  $W_0 = S_0 R(\theta)$ , where  $R(\theta)$  is a parameterized rotation of an auxiliary two-level coin system, and  $S_0 = \exp(i\hat{k}\sigma_z)$  is a coin-dependent translation of the walker [11–13]. Here,  $\sigma_z$  is the Pauli  $z$  operator acting on the coin qubit, and  $\hat{k}$  acts on the walker. In this paper we will take  $R(\theta) = \cos(\theta/2) - i\sin(\theta/2)\sigma_x$ , i.e. a rotation about the  $x$  axis by angle  $\theta$ . The walker operator  $\hat{k}$  can represent momentum, with eigenstates  $|k\rangle$  continuously ranging from 0 to  $2\pi$ . Without loss of generality, we consider the case where the walker initially populates a single  $k$  component, in which case  $\hat{k}$  reduces to a number marking the walker’s position in  $k$  space. At each step, the walker’s position is shifted by  $\pm k$  depending on the coin state.

The single-step quantum walk  $W_0$  is equivalent to the SSH topological-band model in  $k$  space [11], which can be seen by mapping  $W_0$  to a stroboscopic evolution of an effective Hamiltonian, namely  $W_0 = \exp[-iH_{\text{eff}}(k, \theta)]$ ,

with

$$H_{\text{eff}}(k, \theta) = E_{k,\theta} \vec{n}_{k,\theta} \cdot \vec{\sigma}, \quad (1)$$

where  $\vec{\sigma}$  is the vector of the Pauli matrices, and

$$\begin{aligned} \cos E_{k,\theta} &= \cos k \cos \frac{\theta}{2}, \\ \vec{n}_{k,\theta} &= (\cos k \sin \frac{\theta}{2}, -\sin k \sin \frac{\theta}{2}, \sin k \cos \frac{\theta}{2}) / \sin E_{k,\theta}. \end{aligned} \quad (2)$$

$\vec{n}_{k,\theta}$  can be seen to lie on a great circle perpendicular to  $\vec{A} = (0, \cos \frac{\theta}{2}, \sin \frac{\theta}{2})$ . As  $k$  is varied adiabatically from 0 to  $2\pi$ , the number of times  $\vec{n}_{k,\theta}$  winds around the origin is a topological invariant. For  $\theta \neq 0, 2\pi$ , the winding number is 1, as shown in Figs. 1 (a) and (b). Each  $k$  component acquires an identical geometric phase  $\pi$  after a full wind [11]. For  $\theta = 0, 2\pi$ ,  $\vec{n}_{k,\theta}$  coincides with the  $z$  axis, corresponding to the trivial phase, with winding number 0, as shown in Fig. 1 (c).

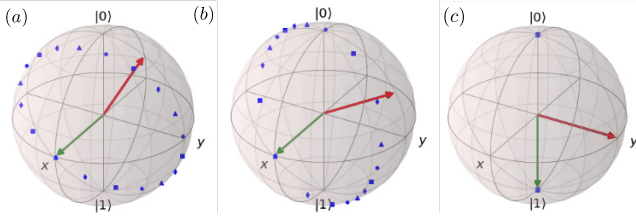


Figure 1. Schematic evolution of  $\vec{n}_k$  (green vector) as  $k$  moves from 0 to  $2\pi$ . (a, b) Topological phase with winding number 1.  $\vec{n}_{k,\theta}$  traces out a great circle (blue dots) perpendicular to  $\vec{A} = (0, \cos \frac{\theta}{2}, \sin \frac{\theta}{2})$  (red vector), as  $k$  runs from  $[0, 2\pi]$ . (a)  $\theta = 2/3\pi$ . (b)  $\theta = 1/3\pi$ . (c) The topologically trivial phase corresponds to  $\theta = 0$ , for which  $\vec{n}_{k,\theta}$  coincides with  $z$  axis and the winding number is 0.

*Step-dependent topological quantum walks.*— To digitally simulate the process of  $k$  translating from 0 to  $2\pi$ , we modify the  $m$ th step unitary as [12, 13, 21]  $W_{\delta k}(m) = S^m W_0$ , where  $S = \exp(i\delta k \sigma_z)$ ,  $\delta k = 2\pi/N$ , with  $N$  an integer. So  $S^m$  shifts  $k$  to  $k + m\delta k$  and, consistent with Eq. (1), we find  $W_{\delta k}(m) = \exp[-iH_{\text{eff}}(k + m\delta k, \theta)]$ . The entire evolution then consists of a sequence of steps from 1 to  $N$ , each step interleaving  $W_0$  and  $S^m$ :

$$W_{\delta k}^{[N,1]} = W_{\delta k}(N)W_{\delta k}(N-1)\dots W_{\delta k}(1). \quad (3)$$

The rotation angle  $\theta$  determines two distinct topological behaviors as  $k$  varies from 0 to  $2\pi$ .

We first consider the topological phase, i.e.  $\theta \neq 0, 2\pi$ . Then, the sequence defined in Eq. (3) is the same as that of adiabatic evolution under the time-dependent Hamiltonian  $H_{\text{eff}}(k + \delta k(t), \theta)$ , with  $H_{\text{eff}}$  defined in Eq. (1) and  $\delta k(t) = \sum_{m=1}^N \Theta(t - m)2\pi/N$ , with  $\Theta$  the step function [12, 13]. The non-trivial topological behavior is connected to the Berry phase acquired by the two-level system (Eq. (1)) during the adiabatic cyclic evolution [22, 23]. As the quantization axis  $\vec{n}_{k,\theta}$

(Eq. (2)) changes adiabatically to  $\vec{n}_{k+\delta k(t),\theta}$ , it traces out a closed path when  $\delta k(t)$  completes a cycle from 0 to  $2\pi$ . Throughout the evolution, the two-level system remains in the same initial superposition of eigenstates with respect to  $\vec{n}_{k+\delta k(t),\theta}$ , but accumulates a geometric phase proportional to the solid angle of the cone subtended by the closed path at the origin. Equation (2) implies that  $\vec{n}_{k,\theta}$  lies on a great circle perpendicular to  $\vec{A}$ . Therefore, each  $k$  state acquires the same geometric phase  $\pi$ . However,  $\vec{n}_{k,\theta}$ -up and  $\vec{n}_{k,\theta}$ -down states have opposite energy  $E_{k,\theta}$ , so they accumulate opposite dynamical phases. To make sure each  $k$  state acquires the same phase  $\pi$ , i.e. refocusing to itself, one has to choose the number of steps  $N$  such that the dynamical phase is modulo  $2\pi$  [12, 13]. The conditions of dynamical phase cancelling and the adiabaticity of the whole process are captured quantitatively by the revival theorem [21],

$$\begin{aligned} ||W_{\delta k}^{[N,1]} + (-1)^{N/2} \mathbb{I}|| &= 2|\cos(\theta/2)|^{N/2}, N \in \text{even}; \\ ||W_{\delta k}^{[2N,1]} + \mathbb{I}|| &= 2|\cos(\theta/2)|^N, N \in \text{odd}; \theta \neq 0, 2\pi, \end{aligned} \quad (4)$$

where  $\theta$  is the rotation angle in the coin toss  $R(\theta)$ , under the condition  $\theta \neq 0, 2\pi$ , i.e. the energy gap  $E_{k,\theta}$  is not closed. When  $N$  is odd ( $N/2$  is even), as long as  $|\cos(\theta/2)| < 1$ , we can find the smallest  $N$  such that  $W_{\delta k}^{[2N,1]} = -\mathbb{I}$  ( $W_{\delta k}^{[N,1]} = -\mathbb{I}$ ) within tolerance.

Next, we consider the topologically trivial case. We take  $\theta = 0$ , which gives  $R(\theta) = \mathbb{I}$  (i.e. the coin is absent). Then Eq. (3) simplifies to a product of  $z$  rotations, giving

$$\begin{aligned} W_{\delta k}^{[N,1]} &= S^{(N+1)N/2} S_0^N, N \in \text{even}; \\ W_{\delta k}^{[2N,1]} &= S_0^{2N}, N \in \text{odd}; \quad \theta = 0. \end{aligned} \quad (5)$$

where we used the fact that  $S^N = \mathbb{I}$  but, in general,  $S^{(N+1)N/2} \neq \mathbb{I}$ . For simplicity, throughout the paper we will take  $N$  to be odd, for which the relative phase between the trivial and the topological case is  $-S_0^{2N}$ , fully controlled by  $S_0$ .

*Matrix embedding.*— We now turn to the implementation of subspace reflections and rotations by considering a system with Hamiltonian which embeds a matrix  $A$  as  $H = \sigma^+ A + \sigma^- A^\dagger$  [24], where  $\sigma^\pm$  are the raising and lowering operators for an auxiliary qubit, and  $A$  has singular value decomposition  $A = \sum_J \Lambda_J |l_J\rangle \langle r_J|$ . Denoting the auxiliary qubit states by  $|0\rangle, |1\rangle$ , in the  $\{|1\rangle |l_J\rangle, |0\rangle |r_J\rangle\}$  basis, we define the walk unitary

$$\begin{aligned} W_0 &:= S_0 \exp(-iHt) = S_0 \exp[-it(\sigma^+ A + \sigma^- A^\dagger)] \\ &= \bigoplus_J S_0 \begin{bmatrix} \cos(\Lambda_J t) |l_J\rangle \langle l_J| & -i \sin(\Lambda_J t) |l_J\rangle \langle r_J| \\ -i \sin(\Lambda_J t) |r_J\rangle \langle l_J| & \cos(\Lambda_J t) |r_J\rangle \langle r_J| \end{bmatrix}. \end{aligned} \quad (6)$$

where  $S_0 = \exp(i\sigma_z k)$ . The evolution  $e^{-iHt}$  plays the role of the coin operator  $R(\theta)$ , where the singular values of  $A$  determine  $\theta/2$ . States that are not coupled to the qubit have singular value zero and thus  $R(\theta) = \mathbb{I}$ . These states correspond to the topologically trivial phase, for which  $W_0$  reduces to  $S_0$ .

The sequence mimicking the topological quantum walk of Eq. (3) now takes the form

$$W_{\delta k}^{[2N,1]} = S^{2N} W_0 \dots S^3 W_0 S^2 W_0 S W_0 \quad (7)$$

$$\cong \bigoplus_J \begin{bmatrix} -|l_J\rangle\langle l_J| & 0 \\ 0 & -|r_J\rangle\langle r_J| \end{bmatrix}, N \in \text{odd}, \quad (8)$$

where  $S = \exp(i\sigma_z 2\pi/N)$  and, due to the revival theorem stated in Eq. (4), the second line holds under the conditions  $|\cos(\Lambda_J t)| < 1$ . Equation (8) shows that when the qubit is initialized in  $|1\rangle$  ( $|0\rangle$ ), the left (right) singular vectors  $|l_J\rangle$  ( $|r_J\rangle$ ) acquire a phase factor  $-1$ . For those states with zero-singular values, by Eq. (5) the phase acquired is determined by the sequence of single-qubit rotations  $S_0^{2N}$ . Thus, we have shown how to rotate a subspace by a given angle assuming a matrix embedded in a larger Hamiltonian. We next demonstrate how fast multiple-controlled-phase gates (reflections) and subspace rotations can be implemented in superconducting circuits, and in the supplementary material we discuss an ion-trap implementation.

*Reflection operations.*—The superconducting-qubit system is composed of a central qubit  $q_0$  and  $N_q$  nearest neighbor qubits, as shown in Fig. 2 (a). Each qubit  $i$  has three energy levels  $|0_i\rangle$ ,  $|1_i\rangle$ ,  $|2_i\rangle$ , with frequency  $\omega_i$ , and  $2\omega_i + \alpha_i$ , where  $\alpha_i$  is the anharmonicity (Fig. 2 (b)). As depicted in Fig. 2 (c), a CZ gate can be applied between ancilla  $q_0$  and any neighbor  $q_j$ , by tuning  $|0_0 2_j\rangle$  into resonance with  $|1_0 1_j\rangle$  [25–28]. We run these CZ gates simultaneously [20] between the ancilla and neighbor qubits in the following implementation.

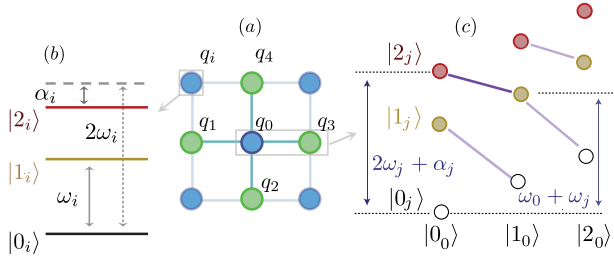


Figure 2. (a) Superconducting qubits (circles) with nearest-neighbor coupling (lines) form a grid lattice. (b) The energy levels of qubit  $i$ .  $|0_i\rangle$  is the ground state and  $|1_i\rangle$  and  $|2_i\rangle$  are the first and second excited states with frequency  $\omega_i$ , and  $2\omega_i + \alpha_i$ , where  $\alpha_i$  is the anharmonicity. (c) CZ gates between qubit 0 and qubit  $j$  through the resonant Rabi oscillation between  $|2_j 0_0\rangle$  and  $|1_j 1_0\rangle$  (dark purple lines). Other transitions (light purple lines) are far off-resonance.

Switching to the interaction picture, which absorbs all the single-qubit phases, the Hamiltonian of the simultaneous gate operation reads,

$$H_q = \sigma_0^{10} \sum_{i=1}^{N_q} g_i \sigma_i^{12} + \sigma_0^{01} \sum_{i=1}^{N_q} g_i \sigma_i^{21}, \quad (9)$$

where  $\sigma_k^{ij} = |i\rangle\langle j|_k$ ,  $g_i$  is the coupling strength between resonant energy levels  $|2_i 0_0\rangle$  and  $|1_i 1_0\rangle$ . We use the rotating wave approximation in Eq. (9), neglecting exchange interaction terms  $\sigma_0^{10} \sigma_i^{01} + \text{H.c.}$  and  $\sigma_0^{21} \sigma_i^{01} + \text{H.c.}$  (the light purple lines in Fig. 2 (c)), which are detuned by  $|\alpha_i|$  and  $|\alpha_i + \alpha_0|$ .

Compared with Eq. (6), the qubit block is defined with respect to the ancilla  $q_0$ , and the embedded matrix is  $A = \sum_i^{N_q} g_i \sigma_i^{12}$ , operating on the neighbors of  $q_0$ . The left singular vectors of  $A$  are the states with at least one qubit in state  $|1\rangle$ . Since we are only interested in computational states, the left singular vectors under consideration are  $|l_J\rangle = |J\rangle$ , for  $J \in \{0, 1\}^{N_q} \setminus \{0\}^{N_q}$ , i.e. non-zero bit strings of length  $N_q$ , where  $J_i$  is the  $i$ th bit from the bit string  $J$ , and  $J_i = 0, 1$  denotes the  $i$ th qubit is in  $|0\rangle$ ,  $|1\rangle$ . Multiplying  $\langle l_J|$  from left with  $A$ , we find the corresponding right singular vectors are  $|r_J\rangle = \sum_{i: J_i=1} g_i / \Lambda_J |J_{\uparrow_i}\rangle$ , where  $\Lambda_J$  is the singular value of  $A$  corresponding to the singular vectors  $|l_J\rangle$ ,  $|r_J\rangle$ , and satisfies  $\Lambda_J^2 = \sum_{i=1}^{N_q} J_i g_i^2$ , where  $J_{\uparrow_i}$  denotes the binary string equal to  $J$ , except on the  $i$ th coordinate where it is equal to 2. Thus,  $|r_J\rangle$  is out of the computational space, and is empty before and after the gate sequence.

Taking the auxiliary  $q_0$  into account, the block Hamiltonian (9) operates as  $H_q |1_0, l_J\rangle = \Lambda_J |0_0, r_J\rangle$ ,  $H_q |0_0, r_J\rangle = \Lambda_J |1_0, l_J\rangle$ , while other states, e.g.  $|0_0, l_J\rangle$ ,  $|1_0, r_J\rangle$  are not affected. Therefore, the evolution is  $\exp(-iH_q t) = \bigoplus_J [\cos(\Lambda_J t) - i \sin(\Lambda_J t) \sigma_x]$ , where  $\sigma_x$  is defined in basis  $|1_0, l_J\rangle$ ,  $|0_0, r_J\rangle$ , and  $\Lambda_J$  is the effective Rabi frequency. This result is consistent with the dynamics of the single-excitation subspace of the inhomogeneous Dicke model with  $\sum_i J_i$  atoms [29, 30], where the harmonic photon mode corresponds to the ancilla  $q_0$ .

The computational space is spanned by  $|l_J\rangle$ , denoting at least one neighbor qubit in  $|1\rangle$ , and  $|\psi_g\rangle = |0_1 0_2 0_3 \dots 0_{N_q}\rangle$  denoting all the neighbor qubits in  $|0\rangle$ . To implement a reflection, the idea is to find a gate time  $t_g$ , such that for all  $J$ , states  $|1_0, l_J\rangle$  acquire the same minus sign due to  $\cos(\Lambda_J t_g) = -1$ . In comparison, states  $|1_0 \psi_g\rangle$  and  $|0_0 x_1 \dots x_N\rangle$ ,  $x \in 0, 1$ , are not affected by Hamiltonian (9). Therefore, provided the ancilla  $q_0$  is initialized in  $|1\rangle$ , the resulting reflection on the neighbor qubits is  $U_{\text{ideal}} = 2|\psi_g\rangle\langle\psi_g| - \mathbb{I}$ . However, such a time  $t_g$  may not exist, since  $\Lambda_J$  varies with how many neighbors are initially flipped to state  $|1\rangle$ , and are generally incommensurate to each other.

The topological walk sequence in Eq. (7) takes  $|1_0, l_J\rangle$  to  $-|1_0, l_J\rangle$ . Therefore, we can implement reflection  $U_{\text{ideal}}$  by interleaving single qubit  $z$  rotations of  $q_0$  and simultaneous two-qubit gate (Hamiltonian  $H_q$  (9)). The sequence defined in Eq. (7) is now replaced with

$$W_0 = S_0 \exp(-iH_q t_g), \quad S = \exp(i\sigma_0^z 2\pi/N). \quad (10)$$

For simplicity, we take  $S_0 = \mathbb{I}$  in which case  $|\psi_g\rangle$  acquires zero net phase (see Eq. (5)). To characterize the perfor-

mance of this approach, we calculate the average gate fidelity by [31]

$$F = \frac{\left| \text{Tr} \left( M U_{\text{ideal}}^\dagger \right) \right|^2 + \text{Tr}(M^\dagger M)}{n(n+1)}, \quad (11)$$

where  $n$  is the dimension of the computational space. Here,  $M = \langle 1_0 | W_{\delta k}^{[2N,1]} | 1_0 \rangle$ , is the unitary operation generated by the matrix element of the qubitized unitary (Eqs. (7, 9, 10)), with initial and final state of  $q_0$  in  $|1\rangle$ .  $M$  is calculated with Qutip [32], where the ancilla  $q_0$  is modeled as a two-level system, and neighboring qubits are three-level systems.

We consider the scenario where  $q_0$  is connected to  $N_q = 4$  neighbors (Fig. 2 (a)). In the case of homogeneous couplings,  $g_i = g$ , we have that  $\Lambda_J/g = \{1, \sqrt{2}, \sqrt{3}, 2\}$ . By Eq. (4), the error is bounded by  $2|\cos(\Lambda_J t_g)|^N$ . We choose  $t_g = 0.333\pi/g$ , such that  $|\cos(\Lambda_J t_g)| \lesssim 0.5$ . With  $N = 3$ , the average gate fidelity  $F = 0.983$ , while  $N = 5$  gives  $F = 0.999$ . Next we take into account inhomogeneous coupling strengths, which may arise from imperfections in fabrication and electronic control. We set  $g_i/g \approx \{0.85, 0.99, 0.91, 1.02\}$ , which are generated by a Gaussian distribution  $\mathcal{N}(1, 0.1^2)$ . By setting  $t_g = 0.333\pi/\max(g_i)$ , the same calculations show we can reach average gate fidelity  $F = 0.999$  with  $N = 7$ .

*Arbitrary rotation of a subspace.*— A key operation in QSVT is the projector-controlled phase shift:  $\Pi_\phi = \exp(i2\phi\Pi)$ . It bestows a phase factor  $e^{i2\phi}$  to the subspace defined by projector  $\Pi$  [2]. Our proposal can be easily adapted to implement  $\Pi_\phi$ , by setting  $S_0 = \exp[i\tilde{\sigma}_0(\pi - 2\phi)/(2N)]$  in Eq. (10). The rotated subspace is then defined by  $\Pi = |\psi_g\rangle\langle\psi_g|$ , i.e. the projection onto the state with all system qubits in  $|0\rangle$ . Note the ancilla is initialized in state  $|1\rangle$  and returns to the same state with probability 1 after an ideal gate operation.

*Discussions.*—We have shown how to implement the multiple-controlled-phase gate  $C_3Z$  (up to a global phase and local transformations) and  $\Pi_\phi$  gate for 4 qubits coupled to a common ancilla. Let us compare the resource cost of our approach with other methods. The total gate time of both  $C_3Z$  and  $\Pi_\phi$  are approximately the same, since we can merge single-qubit rotation  $S_0$  and  $S$ . For homogeneous coupling, taking  $N = 5$  translates to 10 single-qubit rotations of  $q_0$ , and a total time performing simultaneous two-qubit gates of around  $3.33\pi$ , with Rabi frequency  $g$  of the  $|02\rangle \leftrightarrow |11\rangle$  transition set to 1. In contrast, the time to implement a single CZ gate is  $\pi$ . As a benchmark, we consider an efficient  $C_2Z$  gate realization proposed in [33]. In the Supplementary Material, we show how this method can be generalized to implement  $C_{n-1}Z$  at a total CZ gate time cost of  $(2n - 3)\pi$ . The standard realization of 4-qubit  $\Pi_\phi$  requires two rounds of 5-qubit Toffoli gate (locally equivalent to  $C_4Z$ ) surrounding a single-qubit rotation with angle  $\phi$  [1, 2].

In state-of-the-art superconducting processors, a single  $z$  rotation takes roughly 10 ns, and a CZ gate requires around 40 ns [26]. For the 4-qubit  $\Pi_\phi$  gate, our protocol (with homogeneous couplings) thus requires approximately 233 ns to implement, while the scheme of [33] takes  $\approx 570$  ns. However, the method of [33] has the advantage that it is implementable in systems of qubits arranged in a linear chain with nearest-neighbor coupling. Our protocol, on the other hand, is native to star-type connections, where several qubits share a common qubit, and requires shorter overall two-qubit gate time. In comparison with both our method and the method of [33], assuming all-to-all coupling, decomposition of a 4-qubit Toffoli (locally equivalent to  $C_3Z$ ) gate with universal single- and two-qubit gates requires 13 two-qubit gates [8], and comes at a time cost of 520 ns without accounting for the single-qubit gate costs. The 4-qubit  $\Pi_\phi$  requires two rounds of 5-qubit Toffoli gates [1, 2], at even greater expense.

A potential issue with our approach is the dimension of the subspace we can rotate is limited by the connectivity of the auxiliary qubit. As the number of coupled qubits  $N_q$  grows, different effective Rabi frequencies  $\Lambda_J$  distribute over the range from  $g$  to  $\sqrt{N_q}g$ . It could be hard to make  $|\cos(\Lambda_J t_g)|$  simultaneously small across the range of  $\Lambda_J$ , potentially necessitating taking  $N$  large in order to ensure high fidelity. One approach to dealing with this is to view the topological walks of Eq. (3) as a special case of quantum signal processing [4, 5], where the operator  $\exp(-iHt)$  of Eq. (6) is interleaved with single-qubit  $z$  rotations of the ancilla to give  $\prod_{i=1}^{2N} e^{i\phi_i z} e^{-iHt}$ , with vector of  $z$  rotation angles  $\vec{\phi} = (2\pi/N, 4\pi/N, \dots, 4N\pi/N)$ . By carefully choosing different angles  $\vec{\phi}$ , specific polynomial transformations of the singular values of  $A$  can be engineered to give better performance over a wider range of  $\Lambda_J$ . In particular, in the Supplementary Material, we show how a vector  $\vec{\phi}$  of length 10 can be chosen, which allows for subspace reflection of 6 qubits surrounding a central ancilla, with average gate fidelity  $F = 0.999$  and total time less than that required by the  $N = 5$  topological walks method.

*Conclusions and outlook.*—We have proposed an efficient and robust method to implement rotations of a subspace. Compared with conventional decompositions of multiple-controlled-phase gates into single- and two-qubit gates, our proposal offers substantial speedup, enables new ways of compiling algorithms, and can serve as a building block for a wide variety of procedures connected to the QSVT. Our approach is not limited to superconducting circuits, and implementation via Mølmer-Sørensen gates [34] in trapped-ions systems [35, 36] is also possible (see Supplementary Material). Our results hinge on connections between condensed matter physics and quantum information processing, which raises the possibility that further studies on edge states in topolog-

ical quantum walks [11] may provide new perspectives on operations relevant to quantum computing.

## SUPPLEMENTARY MATERIAL

In this supplement, we generalize the  $C_2Z$  gate implementation of [33] to  $n$ -qubits. We provide details on subspace reflections via quantum signal processing and derive the polynomial transformations induced by topological walks. We discuss an ion-trap implementation of our proposal.

### Generalized FSBSW controlled-phase gate

Here, we generalize the  $C_2Z$  gate implementation of Fedorov, Steffen, Baur, da Silva and Wallraff (FSBSW) [33] to  $n$ -qubits, for comparison with our quantum-walk approach.

The general idea of this implementation is to tune state  $|11\rangle$  into resonance with  $|02\rangle$  or  $|20\rangle$ . We denote this resonant Rabi frequency by  $g$ . Other transitions are far off-resonance, as stated in the main text. Since  $|2\rangle$  is out of the computational space, the Rabi oscillation always starts with  $|11\rangle$ . Then at time  $\pi/2g$ ,  $|11\rangle$  will be hidden in the non-computational space by the resonant Rabi oscillation, and is shielded from subsequent operations.

First, let us focus on the area shaded in blue in Fig. 3, which is the same as the gate implementation of [33]. In the blue area, we start with state  $|xx11\rangle$ ,  $x \in 0, 1$ . This state is transferred to  $|xx02\rangle$  when  $gt = \pi/2$ , while the remaining states are unaffected. Then a second gate changes  $|x11x\rangle$  to  $-|x11x\rangle$  when  $gt = \pi$ . Since  $|xx11\rangle$  is first transferred to the non-computational state, we are left with  $|xx00\rangle$ ,  $|xx01\rangle$ ,  $|xx10\rangle$ . So the second gate only imparts a  $\pi$  phase shift to state  $|x110\rangle$ . The third gate swaps  $|xx02\rangle$  back to  $|xx11\rangle$  when  $gt = 3\pi/2$ . In summary, this part bestows a phase shift of  $\pi$  only to state  $|x110\rangle$ .

Now we include the gate operations on the first qubit. State  $|11xx\rangle$  is shielded from subsequent operations by transferring to  $|20xx\rangle$ . In the blue area, we are left with states  $|00xx\rangle$ ,  $|01xx\rangle$ ,  $|10xx\rangle$ . By the previous analysis, only state  $|0110\rangle$  will acquire a minus sign after the operations in the blue area. In the last step, we recover the protected state  $|11xx\rangle$ . So the whole gate sequence in Fig. 3 only takes  $|0110\rangle$  to  $-|0110\rangle$ .

If we apply NOT gates to qubits 2 and 3 in the initial and final stages, the whole sequence shown in Fig. 3 bestows a phase factor -1 only to state  $|0000\rangle$ , which is the same gate operation implemented in the main text.

To add an additional qubit, the trick is to swap state  $|11xxx\rangle$  to the non-computational state  $|20xxx\rangle$  by coupling to the additional qubit. Then the subsequent gate operation only changes  $|x1110\rangle$  to  $-|x1110\rangle$ . This gate

operation can be realized by applying NOT gates to the first qubit before and after the gate sequence shown in Fig. 3. Finally, swapping state  $|11xxx\rangle$  back completes the operation. This five-qubit gate then only changes state  $|01110\rangle$  to  $-|01110\rangle$ . Repeating the above procedure, we can implement a  $C_{n-1}Z$  gate at a total CZ time cost of  $(2n - 3)\pi/g$ .

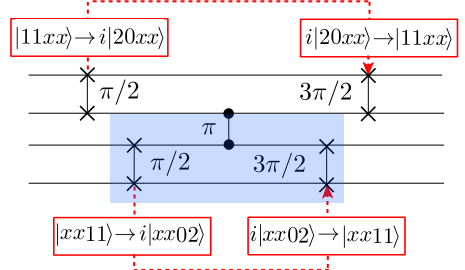


Figure 3. Implementation of the  $C_3Z$  gate based on Ref. [33]. It effects the transformation  $|0110\rangle$  to  $-|0110\rangle$ , with other states unaffected. Each gate is implemented via resonant oscillation between  $|11\rangle$  and  $|02\rangle$  ( $|20\rangle$ ) with times  $\{\pi/2, \pi/2, \pi, 3\pi/2, 3\pi/2\}$  (Rabi frequency  $g$  set to 1).

### Subspace reflection via quantum signal processing

Here we show how quantum signal processing can be used to reflect the subspace spanned by the left eigenstates of  $A$ . This method can be efficiently applied to a larger number (6 vs 4) of qubits than the  $N = 5$  method based on topological walks presented in the main text, and requires less total time to implement with no loss in fidelity. With  $N = 5$ , the topological walk of Eq. (7) with  $S_0 = \mathbb{I}$  effects a degree 10 polynomial transformation of  $\cos(\Lambda_J t)$ , where the polynomial is  $P_{tw}(x) = 2x^{10} - 1$  (see next section).

Consider instead, a different degree  $d = 10$  polynomial

$$P_{a,b}(x) = 2x^2 \frac{(x - a^2)^2(x - b^2)^2}{(1 - a^2)^2(1 - b^2)^2} - 1, \quad (12)$$

with  $a = 0.62, b = 0.3$ . This takes the value 1 at  $x = \pm 1$  and rapidly decays to near -1 away from these two extremes (see Fig. 4). Furthermore,  $P_{0.62,0.3}(x)$  satisfies

1.  $\forall x \in [-1, 1] : |P_{0.62,0.3}| \leq 1$
2.  $\forall x \in (-\infty, -1] \cup [1, \infty) : |P_{0.62,0.3}| \geq 1$
3.  $\forall x \in \mathbb{R} : P_{0.62,0.3}(ix)P_{0.62,0.3}^*(ix) \geq 1$

and thus, by Theorem 4 of [1] there exists  $\vec{\phi} = (\phi_0, \phi_1, \dots, \phi_d)$  such that

$$\langle i | \left[ \prod_{j=1}^d (e^{i\phi_{d+1-j}\sigma_z} W(x)) \right] e^{i\phi_0\sigma_z} | i \rangle = P_{0.62,0.3}(x) \quad (13)$$

where  $i \in \{0, 1\}$  and  $W(x) = \begin{pmatrix} x & -i\sqrt{1-x^2} \\ -i\sqrt{1-x^2} & x \end{pmatrix}$ .

The angles  $\vec{\phi}$  can be found efficiently, e.g. by a method presented in [1], which we compute to be  $\vec{\phi} = (\eta_1, \eta_2, -\eta_2, \eta_1, 0, \eta_1, \eta_2, -\eta_2, \eta_1, 0, 0)$ , where  $e^{i\eta_1} = 0.8718 + 0.4899i$ ,  $e^{i\eta_2} = 0.3831 + 0.9237i$ .

Taking  $x = \cos(\Lambda_J t)$  and comparing to Eq. (6) from the main text shows that, when  $P(\cos(\Lambda_J t)) \approx -1$ , interleaving  $e^{-iHt}$  with single qubit  $z$  rotations with angles given by  $\vec{\phi}$  effects the desired reflection of the (left) singular vectors of  $A$ . Now consider up to 6 qubits each coupled to a central ancilla. With homogenous couplings  $g_i = g$  the singular values of  $A$  satisfy  $\Lambda_J/g \in \{1, \sqrt{2}, \sqrt{3}, 2, \sqrt{5}, \sqrt{6}\}$ . Taking  $t = 0.88/g$  is sufficient to give an average gate fidelity  $F = 0.999$ . Compare this to the topological walk method with  $N = 5$ , which requires the same number (ten) of applications of  $e^{-iHt}$  to achieve  $F = 0.999$  when four neighbouring qubits are coupled to the central ancilla, but each application of  $e^{-iHt}$  is applied for time  $\pi/(3g)$ .

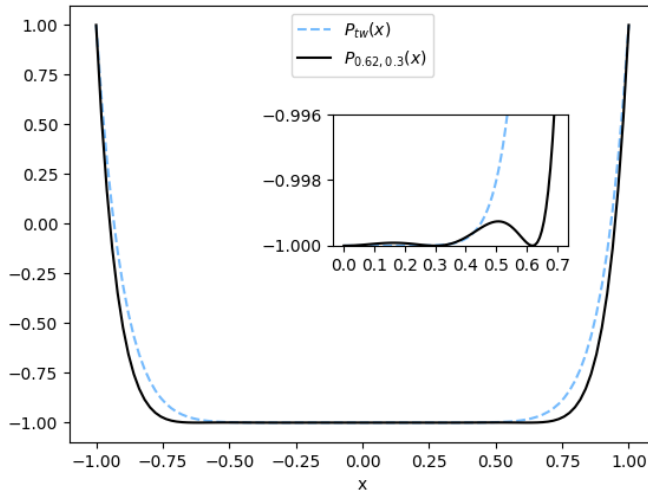


Figure 4. Polynomials  $P_{tw}(x)$  and  $P_{0.62,0.3}(x)$  corresponding to the  $N = 5$  topological walk and the quantum signal processing procedure described in the text, respectively. Inset: close-up of the behaviour of the polynomials in the range  $x \in [0, 0.7]$ .

#### Polynomial transformations induced by topological walks

Let  $N$  be an odd integer. Define  $W(x) = \begin{pmatrix} x & -i\sqrt{1-x^2} \\ -i\sqrt{1-x^2} & x \end{pmatrix}$  and  $R_j = \begin{pmatrix} \omega_j & 0 \\ 0 & \omega_j^* \end{pmatrix}$ , where

$\omega_j = e^{2\pi i j/N}$  for  $j \in \{1, \dots, N\}$ . Define

$$W_N(x) = \prod_{j=1}^N R_{N+1-j} W(x) \quad (14)$$

$$= W(x) \prod_{j=2}^N R_{N+1-j} W(x) \quad (15)$$

where the second line follows from  $R_N = \mathbb{I}$ . The topological walk of Eq. (7) from the main text (with  $S_0 = \mathbb{I}$ ) can then be expressed as

$$W_{\delta k}^{[2N,1]} = [W_N(\cos \Lambda_J t)]^2 \quad (16)$$

Here we show that  $\langle i | [W_N(x)]^2 | i \rangle = 2x^{2N} - 1$ .

From [1],  $W_N(x)$  takes the form

$$W_N(x) = \begin{pmatrix} P(x) & iQ(x)\sqrt{1-x^2} \\ iQ^*(x)\sqrt{1-x^2} & P^*(x) \end{pmatrix} \quad (17)$$

where  $P, Q \in \mathbb{C}[x]$  are polynomials of maximum degree  $N$  and  $N-1$  respectively that satisfy  $|P(x)|^2 + (1-x^2)^2|Q(x)|^2 = 1$  for all  $x \in [1, 1]$ . Furthermore,  $P$  and  $Q$  have parity  $N \bmod 2$  and  $(N-1) \bmod 2$ , respectively.

We now show that  $P(x) = \langle 0 | W_N(x) | 0 \rangle = x^N$ , from which it follows that  $\langle i | [W_N(x)]^2 | i \rangle = 2x^{2N} - 1$ . First note that  $P(x)$  is a polynomial in  $x$  and  $(-i\sqrt{1-x^2})^2$  (see the proof of Lemma 2 of the Supplementary Material of [21]). For real  $x$ , it is therefore invariant to the transformation  $W(x) \mapsto W^*(x)$ . Then, observing that  $R_j = R_{N+2-j}^*$ , we have

$$\langle 0 | W_N(x) | 0 \rangle^* = \langle 0 | W^*(x) \prod_{j=2}^N R_{N+1-j}^* W^*(x) | 0 \rangle \quad (18)$$

$$= \langle 0 | W^*(x) \prod_{j=1}^{N-1} R^j W^*(x) | 0 \rangle \quad (19)$$

$$= \langle 0 | W(x) \prod_{j=1}^{N-1} R^j W(x) | 0 \rangle \quad (20)$$

$$= \langle 0 | [W_N(x)]^\top | 0 \rangle \quad (21)$$

$$= \langle 0 | W_N(x) | 0 \rangle \quad (22)$$

and thus,  $P(x)$  is real. From Lemma 2 of the Supplementary Material of [21], for  $N$  odd, the trace of  $W_N$  satisfies

$$\text{Tr}(W_N(x)) = 2x^N \quad (23)$$

As  $P(x)$  is real, it follows that  $P(x) = x^N$ .

#### Subspace rotations with trapped-ion systems

Here we discuss how our proposal for multi-qubit subspace rotations can be performed in trapped-ion systems [35, 36]. The workhorse in trapped-ion processors is the multi-ion entangling Mølmer-Sørensen (MS)

gate [34], which can entangle up to 24 ions [37]. The unitary operation implemented by the MS gate is parametrized by two angles  $\theta$  and  $\phi$ ,

$$U_{\text{MS}}(\theta, \phi) = \exp \left( -i \frac{\theta}{4} (\cos \phi S_x + \sin \phi S_y)^2 \right), \quad (24)$$

where  $S_{x,y} = \sum_{i=0}^{N_q} \sigma_i^{x,y}$ , with  $\sigma_i^{x,y}$  the Pauli operators acting on the  $i$ th ion. As in the main text, we denote ion number 0 as the ancilla and define [38]

$$\begin{aligned} W_0 &= U_{\text{MS}}(\theta, 0) \exp [i\phi\sigma_0^z] U_{\text{MS}}(\theta, 0) \\ &= \exp \left[ i \frac{\theta}{4} \tilde{S}_x \sigma_0^x \right] \exp [i\phi\sigma_0^z] \exp \left[ -i \frac{\theta}{4} \tilde{S}_x \sigma_0^x \right] \\ &= \exp \left[ i\phi \left( \cos \left( \frac{\theta}{2} \tilde{S}_x \right) \sigma_0^z + \sin \left( \frac{\theta}{2} \tilde{S}_x \right) \sigma_0^y \right) \right], \quad (25) \end{aligned}$$

where we use  $(S_x)^2 = N_q \mathbb{I} + \sum_{ij} \sigma_i^x \sigma_j^x$  and  $\tilde{S}_x = \sum_{i=1}^{N_q} \sigma_i^x$ , i.e. excluding the ancilla.

For any eigenstate  $\tilde{S}_x |\lambda\rangle = \lambda |\lambda\rangle$ , written in the basis  $|0\rangle$  and  $|1\rangle$  of the ancilla, Eq. (25) can be recast in the form,

$$W_0 = \bigoplus_{\lambda} |\lambda\rangle \langle \lambda| \otimes \begin{bmatrix} \cos \phi + i \sin \phi \cos(\frac{\theta \lambda}{2}) & \sin \phi \sin(\frac{\theta \lambda}{2}) \\ -\sin \phi \sin(\frac{\theta \lambda}{2}) & \cos \phi - i \sin \phi \cos(\frac{\theta \lambda}{2}) \end{bmatrix}, \quad (26)$$

where we used  $\exp(-i\theta \vec{n} \cdot \vec{\sigma}/2) = \cos(\theta/2) \mathbb{I} - i \sin(\theta/2) \vec{n} \cdot \vec{\sigma}$ , with  $\vec{n}$  a unit vector, and  $\vec{\sigma}$  the vector of the Pauli matrices.

To implement subspace rotations, we alternate  $W_0$  and  $S = \exp(i\sigma_0^z 2\pi/N)$  as defined in Eq. (7) in the main text. For any non-zero eigenvalue  $\lambda$ ,  $|\cos \phi + i \sin \phi \cos(\frac{\theta \lambda}{2})| < 1$  provided  $\phi \neq 0, \pi$ . So, as guaranteed by the revival theorem [21] in the main text, the topological-walk sequence will bestow a phase  $\pi$  to the subspace corresponding to the non-zero eigenvalues of  $\tilde{S}_x$ .

When  $\lambda = 0$ ,  $W_0 = \exp(i\phi\sigma_0^z) = S_0$ , and thus the zero-eigenvalue subspace will acquire a phase factor  $S_0^{2N}$ , with  $N$  an odd integer, as defined in Eq. (5) in the main text.

Let us take a closer look at the eigenstates of  $\tilde{S}_x$ .  $\tilde{S}_x$  is equivalent to  $\tilde{S}_z = \sum_{i=1}^{N_q} \sigma_i^z$  up to local basis transformation, which has eigenstates satisfying  $\tilde{S}_z |J, M\rangle = M |J, M\rangle$ , with  $M = -J, -J+1, \dots, 0, \dots, J-1, J$ . The maximum value of the angular momentum is  $J = N_q/2$ , and the state  $|N_q/2, \pm N_q/2\rangle$  corresponds to all ions in the same state  $|1\rangle$  or  $|0\rangle$ . In this case, eigenvalue  $M = -N_q/2, -N_q/2+1, \dots, N_q/2$ . Therefore, a zero eigenvalue exists only when the total number of qubits  $N_q$  is even, and the rotated subspace is spanned by the basis with the same number of ions in states  $|1\rangle$  and  $|0\rangle$ , i.e. the zero-eigenvalue subspace. This is slightly different from the circuit-QED implementation in the main text, where the dimension of the rotated subspace is 1, i.e. a subspace spanned by a single state.

\* guxiu1@gmail.com

---

[1] A. Gilyén, Y. Su, G. H. Low, and N. Wiebe, “Quantum singular value transformation and beyond: exponential improvements for quantum matrix arithmetics,” in *Proc. 51st Annu. ACM SIGACT Symp. Theory Comput.* (ACM, New York, NY, USA, 2019) pp. 193–204, [arXiv:1806.01838](https://arxiv.org/abs/1806.01838).

[2] J. M. Martyn, Z. M. Rossi, A. K. Tan, and I. L. Chuang, “A Grand Unification of Quantum Algorithms,” *Quantum* **1**, 1 (2021), [arXiv:2105.02859](https://arxiv.org/abs/2105.02859).

[3] G. H. Low, T. J. Yoder, and I. L. Chuang, “Methodology of Resonant Equiangular Composite Quantum Gates,” *Phys. Rev. X* **6**, 041067 (2016), [arXiv:1603.03996](https://arxiv.org/abs/1603.03996).

[4] G. H. Low and I. L. Chuang, “Optimal Hamiltonian Simulation by Quantum Signal Processing,” *Phys. Rev. Lett.* **118**, 010501 (2017), [arXiv:1606.02685](https://arxiv.org/abs/1606.02685).

[5] G. H. Low and I. L. Chuang, “Hamiltonian Simulation by Qubitization,” *Quantum* **3**, 163 (2019), [arXiv:1610.06546](https://arxiv.org/abs/1610.06546).

[6] D. Poulin, A. Kitaev, D. S. Steiger, M. B. Hastings, and M. Troyer, “Quantum Algorithm for Spectral Measurement with a Lower Gate Count,” *Phys. Rev. Lett.* **121**, 010501 (2018), [arXiv:1711.11025](https://arxiv.org/abs/1711.11025).

[7] R. Babbush, C. Gidney, D. W. Berry, N. Wiebe, J. McClean, A. Paler, A. Fowler, and H. Neven, “Encoding Electronic Spectra in Quantum Circuits with Linear T Complexity,” *Phys. Rev. X* **8**, 041015 (2018), [arXiv:1805.03662](https://arxiv.org/abs/1805.03662).

[8] A. Barenco, C. H. Bennett, R. Cleve, D. P. DiVincenzo, N. Margolus, P. Shor, T. Sleator, J. A. Smolin, and H. Weinfurter, “Elementary gates for quantum computation,” *Phys. Rev. A* **52**, 3457 (1995), [arXiv:9503016](https://arxiv.org/abs/9503016) [quant-ph].

[9] M. Szegedy, “Quantum Speed-Up of Markov Chain Based Algorithms,” in *45th Annu. IEEE Symp. Found. Comput. Sci.* (IEEE, 2004) pp. 32–41.

[10] A. M. Childs, D. Gosset, and Z. Webb, “Universal Computation by Multiparticle Quantum Walk,” *Science* (80-). **339**, 791 (2013).

[11] T. Kitagawa, M. S. Rudner, E. Berg, and E. Demler, “Exploring topological phases with quantum walks,” *Phys. Rev. A* **82**, 033429 (2010), [arXiv:1003.1729](https://arxiv.org/abs/1003.1729).

[12] V. V. Ramasesh, E. Flurin, M. Rudner, I. Siddiqi, and N. Y. Yao, “Direct Probe of Topological Invariants Using Bloch Oscillating Quantum Walks,” *Phys. Rev. Lett.* **118**, 130501 (2017), [arXiv:1609.09504](https://arxiv.org/abs/1609.09504).

[13] E. Flurin, V. V. Ramasesh, S. Hacohen-Gourgy, L. S. Martin, N. Y. Yao, and I. Siddiqi, “Observing Topological Invariants Using Quantum Walks in Superconducting Circuits,” *Phys. Rev. X* **7**, 031023 (2017), [arXiv:1610.03069v1](https://arxiv.org/abs/1610.03069v1).

[14] M. Kjaergaard, M. E. Schwartz, J. Braumüller, P. Krantz, J. I. Wang, S. Gustavsson, and W. D. Oliver, “Superconducting Qubits: Current State of Play,” *Annu. Rev. Condens. Matter Phys.* **11**, 369 (2020), [arXiv:1905.13641](https://arxiv.org/abs/1905.13641).

[15] A. Blais, A. L. Grimsmo, S. M. Girvin, and A. Wallraff, “Circuit quantum electrodynamics,” *Rev. Mod. Phys.* **93**, 025005 (2021), [arXiv:2005.12667](https://arxiv.org/abs/2005.12667).

[16] G. Wendin, “Quantum information processing with superconducting circuits: a review,” *Reports Prog. Phys.* **80**, 106001 (2017), [arXiv:1610.02208](https://arxiv.org/abs/1610.02208).

[17] X. Gu, A. F. Kockum, A. Miranowicz, Y.-X. Liu, and F. Nori, “Microwave photonics with superconducting quantum circuits,” *Phys. Rep.* **718-719**, 1 (2017), [arXiv:1707.02046](#).

[18] P. Krantz, M. Kjaergaard, F. Yan, T. P. Orlando, S. Gustavsson, and W. D. Oliver, “A quantum engineer’s guide to superconducting qubits,” *Appl. Phys. Rev.* **6**, 021318 (2019), [arXiv:1904.06560](#).

[19] J. Q. You and F. Nori, “Atomic physics and quantum optics using superconducting circuits,” *Nature* **474**, 589 (2011).

[20] X. Gu, J. Fernández-Pendás, P. Vikstål, T. Abad, C. Warren, A. Bengtsson, G. Tancredi, V. Shumeiko, J. Bylander, G. Johansson, and A. F. Kockum, “Fast multi-qubit gates through simultaneous two-qubit gates,” [arXiv:2108.11358](#).

[21] C. Cedzich, T. Rybár, A. H. Werner, A. Alberti, M. Genske, and R. F. Werner, “Propagation of Quantum Walks in Electric Fields,” *Phys. Rev. Lett.* **111**, 160601 (2013).

[22] J. J. Sakurai, *Modern Quantum Mechanics* (Addison-Wesley Publishing Company, Inc., 1994).

[23] P. J. Leek, J. M. Fink, A. Blais, R. Bianchetti, M. Goppl, J. M. Gambetta, D. I. Schuster, L. Frunzio, R. J. Schoelkopf, and A. Wallraff, “Observation of Berry’s Phase in a Solid-State Qubit,” *Science* (80- ). **318**, 1889 (2007).

[24] S. Lloyd, B. T. Kiani, D. R. M. Arvidsson-Shukur, S. Bosch, G. De Palma, W. M. Kaminsky, Z.-W. Liu, and M. Marvian, “Hamiltonian singular value transformation and inverse block encoding,” [arXiv:2104.01410](#).

[25] F. W. Strauch, P. R. Johnson, A. J. Dragt, C. J. Lobb, J. R. Anderson, and F. C. Wellstood, “Quantum Logic Gates for Coupled Superconducting Phase Qubits,” *Phys. Rev. Lett.* **91**, 167005 (2003).

[26] R. Barends, J. Kelly, A. Megrant, A. Veitia, D. Sank, E. Jeffrey, T. C. White, J. Y. Mutus, A. G. Fowler, B. Campbell, Y. Chen, Z. Chen, B. Chiaro, A. Dunsworth, C. Neill, P. O’Malley, P. Roushan, A. Vainsencher, J. Wenner, A. N. Korotkov, A. N. Cleland, and J. M. Martinis, “Superconducting quantum circuits at the surface code threshold for fault tolerance,” *Nature* **508**, 500 (2014).

[27] V. Negîrneac, H. Ali, N. Muthusubramanian, F. Battistel, R. Sagastizabal, M. S. Moreira, J. F. Marques, W. J. Vlothuizen, M. Beekman, C. Zachariadis, N. Haider, A. Bruno, and L. DiCarlo, “High-Fidelity Controlled-Z Gate with Maximal Intermediate Leakage Operating at the Speed Limit in a Superconducting Quantum Processor,” *Phys. Rev. Lett.* **126**, 220502 (2021), [arXiv:2008.07411](#).

[28] Y. Sung, L. Ding, J. Braumüller, A. Vepsäläinen, B. Kannan, M. Kjaergaard, A. Greene, G. O. Samach, C. McNally, D. Kim, A. Melville, B. M. Niedzielski, M. E. Schwartz, J. L. Yoder, T. P. Orlando, S. Gustavsson, and W. D. Oliver, “Realization of High-Fidelity CZ and ZZ-Free iSWAP Gates with a Tunable Coupler,” *Phys. Rev. X* **11**, 021058 (2021), [arXiv:2011.01261](#).

[29] A. B. Klimov and S. M. Chumakov, *A Group - Theoretical Approach to Quantum Optics* (Wiley, 2009).

[30] O. Tsypliyatayev and D. Loss, “Classical and quantum regimes of the inhomogeneous Dicke model and its Ehrenfest time,” *Phys. Rev. B* **82**, 024305 (2010).

[31] M. A. Nielsen, “A simple formula for the average gate fidelity of a quantum dynamical operation,” *Phys. Lett. A* **303**, 249 (2002), [arXiv:0205035](#) [[arXiv:quant-ph](#)].

[32] J. R. Johansson, P. D. Nation, and F. Nori, “QuTiP: An open-source Python framework for the dynamics of open quantum systems,” *Comput. Phys. Commun.* **183**, 1760 (2012).

[33] A. Fedorov, L. Steffen, M. Baur, M. P. da Silva, and A. Wallraff, “Implementation of a Toffoli gate with superconducting circuits,” *Nature* **481**, 170 (2011).

[34] K. Mølmer and A. Sørensen, “Multiparticle Entanglement of Hot Trapped Ions,” *Phys. Rev. Lett.* **82**, 1835 (1999).

[35] C. Monroe, W. C. Campbell, L.-M. Duan, Z.-X. Gong, A. V. Gorshkov, P. W. Hess, R. Islam, K. Kim, N. M. Linke, G. Pagano, P. Richerme, C. Senko, and N. Y. Yao, “Programmable quantum simulations of spin systems with trapped ions,” *Rev. Mod. Phys.* **93**, 025001 (2021), [arXiv:1912.07845](#).

[36] C. D. Bruzewicz, J. Chiaverini, R. McConnell, and J. M. Sage, “Trapped-ion quantum computing: Progress and challenges,” *Appl. Phys. Rev.* **6**, 021314 (2019), [arXiv:1904.04178v1](#).

[37] I. Pogorelov, T. Feldker, C. D. Marciniak, L. Postler, G. Jacob, O. Kriegelsteiner, V. Podlesnic, M. Meth, V. Negnevitsky, M. Stadler, B. Höfer, C. Wächter, K. Lakhmanskiy, R. Blatt, P. Schindler, and T. Monz, “Compact ion-trap quantum computing demonstrator,” *PRX Quantum* **2**, 020343 (2021).

[38] M. Müller, K. Hammerer, Y. L. Zhou, C. F. Roos, and P. Zoller, “Simulating open quantum systems: from many-body interactions to stabilizer pumping,” *New J. Phys.* **13**, 085007 (2011).